A CURRENT ANALYSIS AND CORRECTION SYSTEM FOR VIBRATION FORCES ON THE ROTOR OF A ROTATING ACTIVE MAGNETIC BEARING SYSTEM

R. Gouws and G. van Schoor

School of Electrical, Electronic and Computer Engineering, North-West University, Private Bag X6001, Potchefstroom, 2520, South Africa

Abstract: In this paper, an on-line detection, correction and identification system for vibration forces on the rotor of a rotating active magnetic bearing is proposed. The on-line detection system performs current analysis by comparing ideal no fault currents with fault currents. Pattern recognition was performed by using an input feature obtained from the Wigner-Ville distribution and by comparing fault current patterns with historical fault database patterns obtained from a fully suspended 250 kW water cooling active magnetic bearing pump. A fuzzy logic system used the output of the pattern recognition process to perform error correction on the active magnetic bearing system. A fault identification system provides the type of fault, where the fault occurred in the active magnetic bearing system, the current state of the rotor and the parameters of the fault. Experiments were performed on a double radial active magnetic bearing test rack to demonstrate the effectiveness of the proposed system in the detection, correction and identification of vibration forces on the rotor of an active magnetic bearing system. The detection, diagnosis and correction system corrected and minimised vibration forces to a stable working condition.

Key words: Active magnetic bearing, control, diagnostics, vibration monitoring, pattern recognition, simulation.

NOMENCLATURE

A_e_1	Amplitude of fault
A_i_1	Current 1 amplitude
A_{fit}	Accuracy of the fit with the data
B_e_1	Frequency of fault
C_e_1	Phase of fault
D_e_1	Offset of fault
D_i_1	Current offset
e_{d1}	Diagnosis output error
e_{fuz1}	Fuzzy current 1 error
e_{i1}, e_{i2}	Errors for current 1 and current 2
e_{i1_ref}	Historical database error 1
e_{i2_ref}	Historical database error 2
F_{data}	Historical fault data
f_1, f_2	Force for the top and bottom electromagnets
f_3, f_4	Carrier and vibration forces on the rotor
i_{1_mask}	Masked current 1
i_{ref_1R}	Relation for reference current 1
i_{ref_2R}	Relation for reference current 2
i_{ref}, i_o	Reference and bias currents
i_{ref_1}, i_{ref_2}	Reference currents (top and bottom bearings)
i_1, i_2	Current in top and bottom electromagnets
K_p, K_i, K_D	PID controller gains
t_c, t_r	Cycling and running time
x_p, x_{pref}	Actual and reference displacements

1. INTRODUCTION

Active magnetic bearings (AMBs) are bearings where the suspension forces for supporting the rotor are generated magnetically without any contact. AMBs are inherently unstable and control is required to levitate the rotor. Compared with ball bearings, AMBs have the advantage of no contact and lubrication, which allows for high-speed rotation. AMBs can be applied to high-speed rotating machinery like turbo pumps [1], flywheels for energy storage [2] and turbo compressors [3].

The bearings of an AMB are equipped with sensors and actuators, which provide the exact displacement and current values during machine operation. This makes AMBs ideally suited for condition monitoring, diagnosis and correction.

This project focuses on using the available sensors and actuators to perform current analysis. An on-line detection, diagnosis and correction system was developed that performed the current analysis process and induced correctional forces on the rotor of the rotating AMB system. The detection system constitutes current masking and feature extraction performed by the Wigner-Ville distribution (WVD). The diagnosis and correction system constitutes pattern recognition and fuzzy logic.

For this project it was necessary to use two AMB systems. The first was a fully suspended 250 kW water cooling AMB pump (shown in Figure 27) on which condition monitoring was performed over a period of three years to obtain historical fault data. The water cooling AMB pump is a fully working system and it was not possible to make any changes to the system.

A second AMB system, the double radial AMB test rack (diagram shown in Figure 1) was used for verification purposes. This system constitutes a driven unit with magnetic bearings and position sensors on both sides. The controllers use the position of the shaft to provide actuating signals to the power amplifiers, which in turn

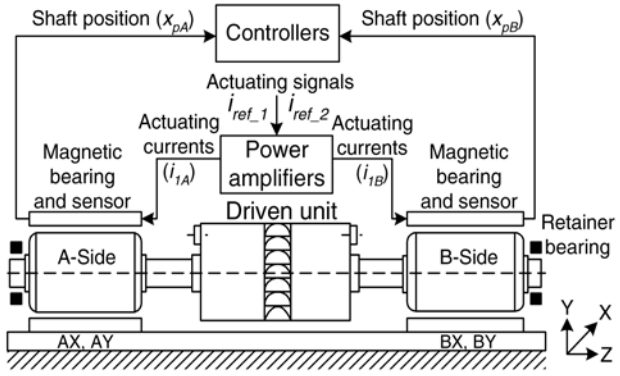

Figure 1: Double radial AMB system.

provide the magnetic bearings with the correct current to suspend the shaft. The specifications of this system are provided in Table IV.

Diagnosis of AMB systems can be performed by means of a signal-based approach, which relies on the analysis of the displacement and current signals and by means of a model-based approach, which utilizes a mathematical model of the system [4]-[6].

A combination of signal-based analysis and model-based analysis was performed during the development process of the on-line diagnosis and correction system.

The first step in the design process of the on-line diagnosis and correction system was to evaluate the vibration forces that occurred on the 250 kW water cooling AMB pump and to develop a system capable of detecting these vibration forces. The second step was to diagnose the vibration forces and extract features. The last step was to use the features to correct the vibration forces. This process is detailed in Section 3.

An identification system was developed that provided the type of fault, where the fault occurred, the current state of the fault, the parameters of the fault and the day and time when the fault first occurred. This system constitutes fault data fitting and frequency pattern comparison, detailed in Section 3.4.

2. VIBRATION FORCES ON THE ROTOR

The following section provides an overview of the vibration forces on the rotor of the 250 kW water cooling AMB pump. Historical fault data have been captured by performing condition monitoring on the current signals over a period of 3 years. Error signals were then calculated for each of the historical data sets and the signals were used as input to the simulation and practical AMB models (detailed in Section 3.1). This was done to induce the same vibration (disturbance) forces that occurred on the water cooling AMB pump on the double radial AMB test rack.

It became evident from the historical fault data of the water cooling AMB pump that vibration forces can be categorised into the following three fault categories: 1) low frequency, 2) medium frequency and 3) high frequency. Low frequency faults refer to vibration forces with frequencies lower than the carrier frequency of the rotor, medium frequency to frequencies very close to the carrier frequency and high frequency to frequencies higher than the carrier frequency (Ω) of the rotor.

2.1 Historical fault dataset 1: Low frequency faults

Faults causing low frequency vibrations on the rotor of the 250 kW water cooling AMB pump occurred due to vibrations from machines running at low rotational speeds in the vicinity.

2.2 Historical fault dataset 2: Medium frequency faults

Faults causing medium frequency vibrations on the rotor of the 250 kW water cooling AMB pump occurred due to temperature growth of the machine structure, shifting of the relative position of components after assembly and the coupling face not being perpendicular to the shaft axis.

Further vibrations occurred due to excessive force of the water against the pump blades, during excessive valve opening and closing. The faults in this dataset were either characterised as misalignments or as unbalances. Load unbalances and misalignments are well documented for high-speed turbines where loss of compressor or turbine blades, though uncommon, can occur [7].

2.3 Historical fault dataset 3: High frequency faults

Faults causing high frequency vibrations on the rotor of the 250 kW water cooling AMB pump occurred due to loose bolts on the motor side, which caused vibration forces in the motor that was carried onto the shaft of the AMB pump.

Further vibrations occurred due to external vibrations from machines running at high rotational speeds in the vicinity. The faults in this dataset were mostly characterised as foundation looseness faults. Foundation looseness or motion of the system base, on which the bearings are mounted, can occur in various applications [8].

3. SYSTEM DEVELOPMENT

This section explains the system development process of the on-line detection, diagnosis and correction system. A process diagram of the vibration and correction forces is shown in Figure 2. At start up the AMB system is suspended only with PID controllers and rotated at the desired speed of 1000 rpm. Current masking is performed during this initial period when no vibration forces are occurring on the system. The rotational speed of the rotor is used as input to the current masking process. The masked current is stored to memory.

When a vibration force occurs on the rotor, the system detects the fault and calculates the vibration error, frequency and pattern. The stored no fault current is used to calculate the vibration error. Data fitting is then performed on the vibration error and the masked current.

The fault identification system identifies the fault according to the result obtained from the data fitting,

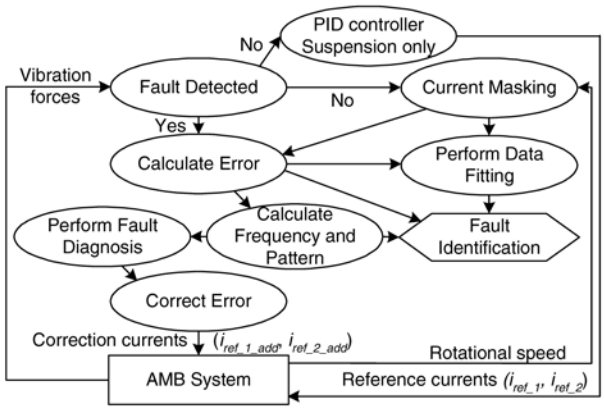

Figure 2: Process diagram: vibration and correction forces.

vibration error, frequency and pattern. The frequency and pattern are sent to the fault diagnosis and error correction systems, which calculate the correction currents needed to stabilise the rotor.

The rotor view of the vibration and correctional forces, where the PID controller fails to correct the vibrations is shown in Figure 3. In this diagram a vibration force causes the rotor to suddenly move to the upward right corner. Without immediate correction the rotor will crash against the retainer bearings and cause damage to the system.

Correction forces are applied on the rotor by increasing or decreasing the reference currents i_{ref_1} and i_{ref_2} according to the direction of the vibration force. The on-line detection, diagnosis and correction system performs the calculations for the correction forces.

Figure 4 provides an overview of the detection, diagnosis and correction system that was implemented on the double radial AMB test rack. The fault detection subsystem uses the currents i_1 and i_2 to detect the vibration forces on the AMB system and calculates the current errors e_{i1} and e_{i2}, through a process of current masking and error calculation. The fault detection system is explained in Section 3.2.

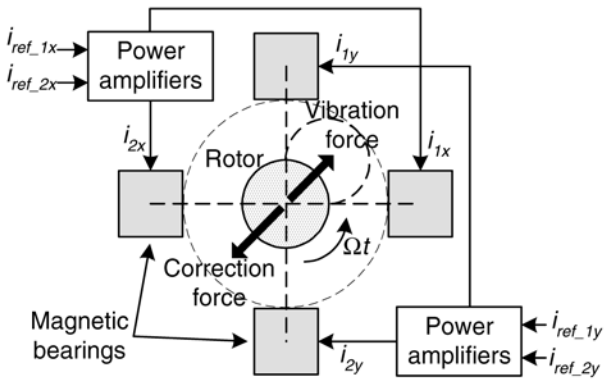

Figure 3: Illustration of the vibration and correctional forces.

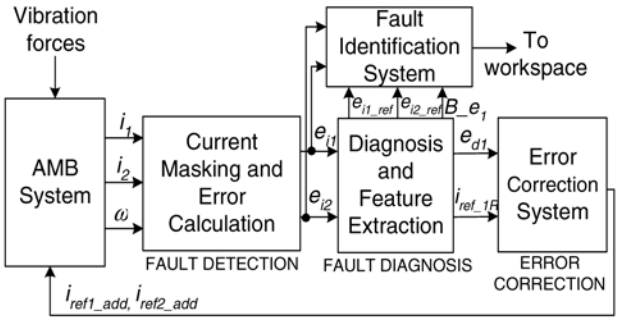

Figure 4: Overview: detection, diagnosis and correction system.

After a fault has been detected, the error signals (e_{i1} and e_{i2}) are sent to the fault diagnosis system where feature extraction is performed. The fault diagnosis system is explained in Section 3.3.

The error correction system uses the diagnosis output error (e_{d1}) and the workforce relation current (i_{ref_1R}) as features to stabilise the rotor by inducing correction forces on the rotor. The error correction system is explained in Section 3.3.

The parameters $i_{ref\_1\_add}$ and $i_{ref\_2\_add}$ represent the correction reference currents for the top and bottom magnetic bearings, respectively.

The fault identification system uses the current errors (e_{i1} and e_{i2}), historical database errors (e_{i1_ref} and e_{i2_ref}) and the frequency (B_e_1) to identify the type of vibration force. The fault identification system is explained in Section 3.4.

3.1 Simulation and practical AMB models

A simulation model of the AMB system was necessary to observe how the practical system will respond to faults, when the diagnosis and correction system is implemented. Figure 5 provides the simulation (dashed and solid lines) and practical (solid lines) models of the rotating double radial AMB system with vibration forces.

The actual position (x_p) is subtracted from the reference position to provide the position error (e_p). This is fed to a PID controller which together with the bias current (i_0) provides the reference currents (i_{ref_1} and i_{ref_2}) for the power amplifiers. The forces (f_1 and f_2) are calculated with $(K_m \cdot i_1^2)/x_p^2$ and $(K_m \cdot i_2^2)/(g_t)^2$, where K_m is the constant of the magnetic bearing and g_t is the total air gap. The position (x_p) is obtained by double integrating the forces and dividing the answer with the mass of the rotor (m).

For the simulation model, the vibration force (f_4) on the rotor was induced by subtracting the position error (e_p) from the reference error index ($e_{ref} \cdot \sin(\omega_2 t)$) and feeding this to a controller. The reference error (e_{ref}) represents the error calculated from the historical fault data of the

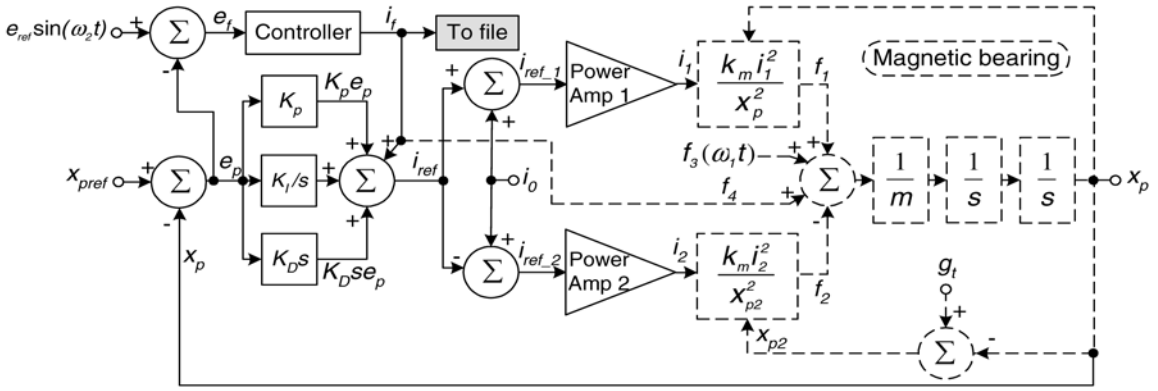

Figure 5: Simulation (dashed and solid lines) and practical (solid lines) AMB models with rotational rotor faults.

water cooling AMB pump and the index ($\sin(\omega_2 t)$) represents the carrier of the AMB pump.

The output of the controller is then added as a reference force (f_4) and the connection to add a reference current fault (i_f) to the reference current (i_{ref}) is disconnected. The carrier force ($f_3(\omega_1 t)$) of the double radial AMB was kept constant and the vibration force (f_4) was stored to file. The stored file now contains both the carriers of the water cooling AMB pump and the double radial AMB test rack.

The file was then demodulated to subtract the carrier of the water cooling AMB pump and the remainder was used to simulate vibration forces on the rotor. These vibration forces (f_4) are synchronously placed on the carrier of the double radial AMB test rack.

For the practical AMB system the connection to add a reference current fault (i_f) to the reference current (i_{ref}) is restored and the vibration force (f_4) is disconnected.

The reference current fault (i_f) is then stored to file, during the controlling process of the rotating double radial AMB test rack. The file is demodulated to subtract the carrier of the water cooling AMB pump and the remainder is used as reference current faults to induce vibration forces on the rotor. These reference current faults (i_f) are synchronously placed on the carrier of the double radial AMB test rack.

3.2 Fault detection system

The fault detection system (shown in Figure 6) constitutes current masking, error calculation and frequency calculation. Current masking is performed by capturing

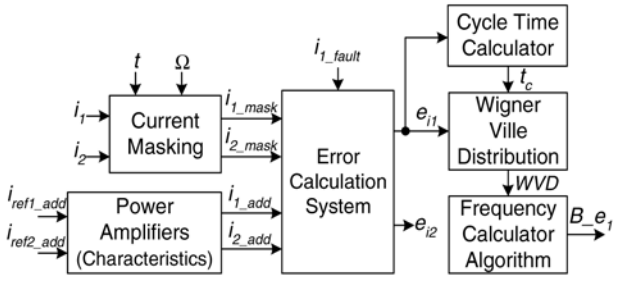

Figure 6: Fault detection system.

one cycle of the current (i_1) during a no fault condition of the AMB system. A sine wave representation of the no fault current (i_{1_mask}) is obtained and stored to memory. This process is done only once and when no vibration force is occurring on the system. When a fault occurs in the system, the current (i_1) is called the fault current (i_{1_fault}). The no fault current (i_{1_mask}) is subtracted from the fault current (i_{1_fault}) to provide the current error (e_{i1}). When there is a sudden change in the rotational speed (Ω) of the rotor, the frequency of the no fault current (i_{1_mask}) is changed to compensate for the change. The current masking process during the practical implementation process is discussed in Section 4.

When a vibration force occurs in the AMB system, the detection, diagnosis and correction system corrects the fault by applying correctional forces to the shaft. These correctional forces are applied by adding correctional reference currents (i_{ref1_add} and i_{ref2_add}) to the existing reference currents (i_{ref_1} and i_{ref_2}). When the correctional reference currents are applied the actual currents (i_1 and i_2) change. To retain the initial error information prior to the error correction the error correction currents need to be subtracted from the resulting currents of the corrected system. In this manner a change in error conditions will be sensed and appropriately corrected by a change in the error correction currents.

The Wigner-Ville distribution (WVD) was developed to overcome a limitation of the Short-Time Fourier Transform (STFT), where high-resolution cannot be obtained simultaneously in both time and frequency domains [9]. The WVD was developed to utilise the Fourier transform in a similar way and due to this similarity the WVD has been interpreted as a modified version of the STFT [10].

Data point number reduction is not necessary during the time-shifting operation of the WVD process. The process is started with the Fourier transform of the ensemble-average instantaneous correlation product as shown in the following equation:

$$FT(x(t)) = \int_{-\infty}^{+\infty} E\left(x(t+\frac{\tau}{2}) x^{*}(t-\frac{\tau}{2}) \right) e^{-j2\pi\nu\tau} d\tau \qquad (1)$$

where x^* is the conjugate of x for complex signals or Hilbert transform of x for real signals which, in theory, is

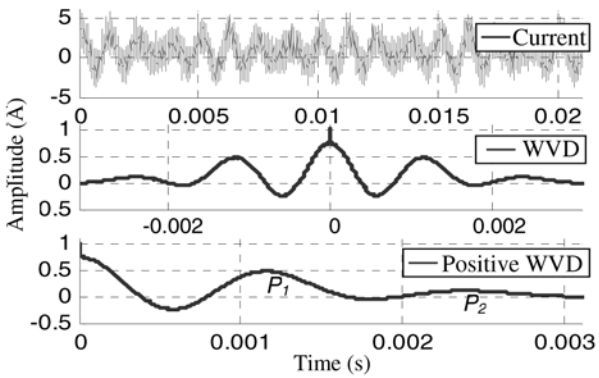

Figure 7: Frequency calculation with the WVD.

a measure of the frequency content of a non-stationary random process *x(t)* [11]-[12].

It is not possible to compute the ensemble-average function accurately in practice, because of the infinite number of data required. One solution to deal with the non-stationary case is to omit the ensemble-average in Equation 1:

$$WVD(x(t,v)) = \int_{-\infty}^{+\infty} x(t+\frac{\tau}{2})x^{*}(t-\frac{\tau}{2})e^{-j2\pi v\tau}d\tau \qquad (2)$$

The WVD is very often used in practical applications, since it avoids interference between positive and negative frequencies [10]. The properties of the WVD have been studied extensively over the past 15 years [13]. It has been shown that the WVD fulfils the greatest number of theoretical and practical properties within the class of time-frequency distributions [14]. The WVD always goes to zero at the beginning and end of finite-duration signals [15]. The discrete representation for Equation 2 is:

$$WVD(x(T_S,v)) = \frac{T_S}{\pi}\sum_{k=-\infty}^{+\infty} x^{*}(t-kT_S)x(t+kT_S)e^{-2ivkT_S} \qquad (3)$$

where T_s is the sampling period and must be chosen so that

$T_s \quad (\pi/2\omega_{max})$ and ω_{max} is the highest frequency in a random signal.

The WVD was calculated by using Equation 3 and the frequency (B_e_1) was calculated from the WVD and a frequency calculator algorithm. The accuracy of the frequency was improved by sampling the WVD at two times the cycle time (t_c) of the error signal (e_{i1}).

The WVD is calculated from the current error (e_{i1}) and the peaks P_1 and P_2 are calculated from the positive peaks of the WVD as shown in Figure 7. From peak P_1 the frequency of the fault was calculated at 854.7 Hz. This frequency calculation is only for illustrational purposes.

It can be seen from Equation 4 that the second peak (P_2) is a multiple of the first peak. The value calculated in this equation provides an estimate of the error factor on the first peak (P_1). In this case the frequency calculated has 99.15 % accuracy.

$$\frac{P_2}{P_1} = \frac{2.36\times10^{-3}}{1.17\times10^{-3}} = 2.017 \qquad (4)$$

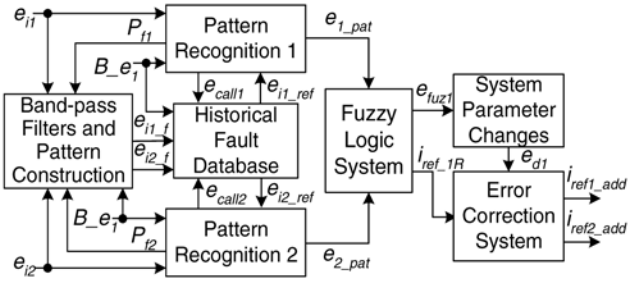

Figure 8: Fault diagnosis and correction system.

3.3 Fault diagnosis and correction systems

This section discusses the fault diagnosis and correction system, shown in Figure 8. The pattern recognition 1 and 2 subsystems compare the current errors (e_{i1} and e_{i2}) of the on-line system with the reference current errors (e_{i1_ref} and e_{i2_ref}) of the historical fault database. The pattern recognition 1 and 2 subsystems call (e_{call1} and e_{call2}) the reference current errors from the database at a specific frequency (B_e_1).

When a fault occurs without a recognisable pattern, the pattern is band-pass filtered (centre frequency being the error frequency (B_e_1)) and stored to the historical fault database.

Figure 9 shows the process diagram of the pattern recognition subsystem. The system tests the difference between the on-line current errors (e_{i1} and e_{i2}) and the reference current errors (e_{i1_ref} and e_{i2_ref}) from the historical fault database. If the error difference is big, the error obtained from the on-line AMB system is used for correctional purposes. At this stage no recognisable pattern exists and the pattern construction system constructs and stores a new pattern.

When the error difference is small (close to zero), the system calculates the frequency and closest pattern to the available on-line data. If the frequency stays constant, the system uses the closest pattern to correct the fault. If the frequency changes the system tests the data in the historical fault database for a possible combination pattern. When no combination of the available data is found, the system uses the on-line error to correct the

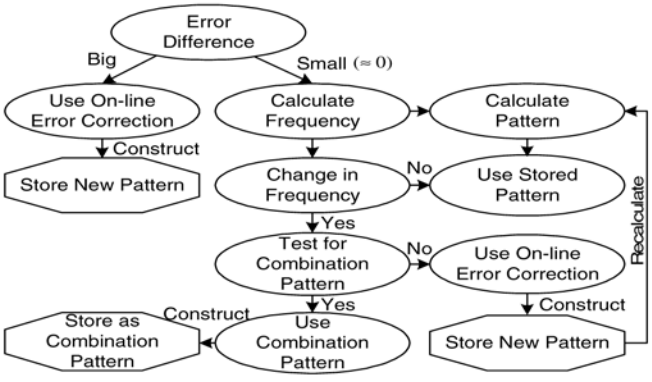

Figure 9: Process diagram: pattern recognition subsystem.

fault. A new pattern is constructed and stored to the database and the pattern calculation process is repeated.

If the system finds a combination pattern, the system uses the pattern and stores the pattern as a combination pattern.

The construction subsystem constructs and stores new patterns (e_{i1_f} and e_{i2_f}) according to the fault signals (e_{i1} and e_{i2}), when it receives pattern faults (P_{f1} and P_{f2}) from the pattern recognition subsystems.

The more faults occur in the system, the more new correctional data become available. The system is able to switch between different patterns and train itself to react to faults that are a combination of the available fault data. An orbital representation of the currents (i_{1x} and i_{1y}) and three low frequency correctional patterns can be seen in Figure 10. Pattern low_{new} is a trained pattern which consists of pieces of three low frequency correctional patterns low_1, low_2 and low_3.

The pattern (low_{new}) was stored as a combination pattern and decreased the vibration forces on the rotor of the AMB system. For each of the patterns in the historical fault database there exist a frequency and description.

Figure 11 provides the fuzzy membership functions for pattern error 1 (e_{1_pat}) and pattern error 2 (e_{2_pat}). Fuzzification is performed by using the overlapping fuzzy sets bad negative (B-), good (G) and bad positive (B+). The basic rule for using the features (e_{1_pat} and e_{2_pat}) is: IF e_{1_pat} AND e_{2_pat} THEN e_{fuz1}. The same rule applies for variable i_{ref_1R}. Table I provides the rule matrix for fuzzy1 current error e_{fuz1} and relation current i_{ref_1R}.

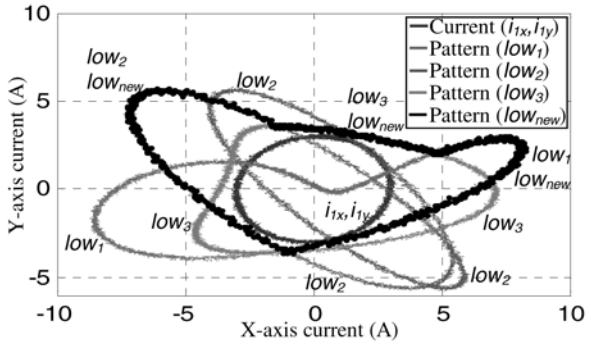

Figure 10: Orbital representation: low frequency pattern errors

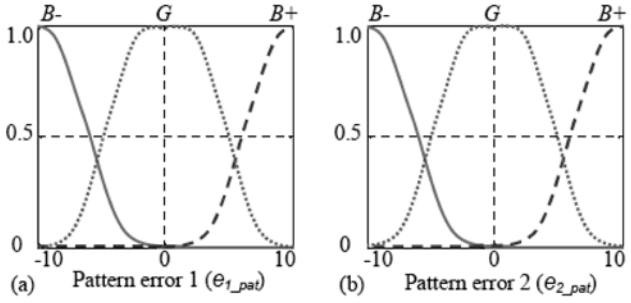

Figure 11: Fuzzy membership function for (a) pattern error 1 (e_{1_pat}) and (b) pattern error 2 (e_{2_pat}).

Table I: Rule matrix for fuzzy current error (e_{fuz1}) and relation current (i_{ref_1R})

e_{fuz1}, i_{ref_1R}		e_{1_pat}		
		B+	G	B-
e_{2_pat}	B+	P, B	M, B	M, B
	G	M, B	M, M	M, B
	B-	M, B	M, B	N, T

The fuzzy surface plots for fuzzy1 current error (e_{fuz1}) and relation current 1 (i_{ref_1R}) are shown in Figure 12 and Figure 13, respectively. Defuzzification of the fuzzy membership functions e_{fuz1} and i_{ref_1R} are performed by using overlapping fuzzy sets negative (N), middle (M) and positive (P) and bottom (B), middle (M) and top (T), respectively.

When a vibration force causes the rotor to move downward, the reference current 1 (i_{ref_1}) needs to be more than reference current 2 (i_{ref_2}) to stabilise the rotor to the centre position.

This relation between the amplitude of the vibration force and amount of current required by each amplifier are called the workforce relation current and is defined by i_{ref_1R} and i_{ref_2R}. i_{ref_1R} refer to the workforce relation current for the top power amplifier and i_{ref_2R} refer to the workforce relation current for the bottom power amplifier.

Workforce relation current 2 (i_{ref_2R}) is calculated as follows:

$$i_{ref\_2R} = 1.1 - i_{ref\_1R} \tag{5}$$

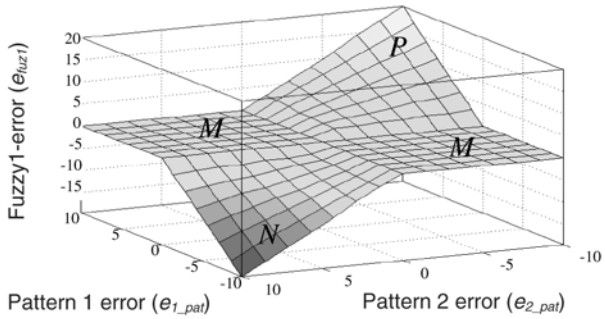

Figure 12: Fuzzy surface plot for fuzzy1 current error (e_{fuz1}).

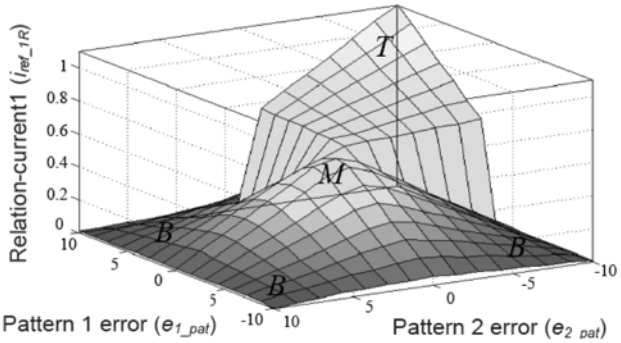

Figure 13: Fuzzy surface plot for relation current 1 (i_{ref_1R}).

The workforce relation current serves as an amplifier (booster) and increases or decreases the amplitude of the correction force according to the error made on the current. These increases and decreases of the correct amplifiers, causes faster correction force response times.

System parameter changes of amplitude change and phase shifting are performed on the fuzzy1 current error (e_{fuz1}), before sent to the error correction system. The fuzzy current error is then called the diagnosis output error (e_{d1}).

Correctional reference 1 current is calculated as follows:

$$i_{ref1\_add} = i_{ref\_1R} * e_{d1} \quad (6)$$

The correctional reference 1 current is added to reference current 1 (i_{ref_1}). Correctional reference 2 current is calculated as follows:

$$i_{ref2\_add} = -i_{ref\_2R} * e_{d1} \quad (7)$$

The correctional reference 2 current is added to reference current 2 (i_{ref_2}).

3.4 Fault identification system

Figure 14 provides the process diagram of the fault identification system. When no fault is detected, the identification system provides no output. When a fault is detected, the system uses the frequency to determine to which frequency dataset (low, medium or high) the fault belongs. The system performs data fitting to calculate the best possible fit of the historical fault data in the specific dataset with the data obtained from the practical AMB system.

If the frequency rapidly changes from one dataset to another, the system saves the output, predicts the closest type of fault (unbalance, misalignment, foundation looseness or as otherwise specified in the historical fault database) and recalculates the fault in the new dataset.

When the frequency stays within a certain dataset, the system is set to repeatedly calculate the average error over a time period of 1 second. The time period was calculated at five times the period of the masked current at 1000 rpm. The type of fault is given to the fault in the dataset with the smallest error over the available time period.

After the type of fault is stored, the system displays the parameters of the fault and determines the current state of the fault. The current state of the fault is calculated from the maximum current output of the power amplifiers. The system determines the side and axis where the fault occurs from the current error signals.

Faults are allocated to the A-side and B-side and can occur in the x, y and z axes. The identification system was limited to the A-side and the y-axis, due to the installation of the roller bearing on the B-side and the limitation in the sampling time of the dSPACE® controller. The day and time when the fault first occurred is saved and displayed.

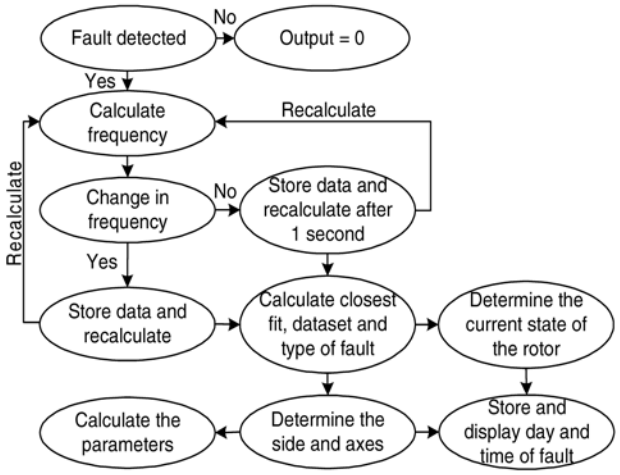

Figure 14: Process diagram of the identification system.

Figure 15 shows the parameter diagram of the fault identification system used to calculate the type of fault, where the fault occurs, current state of the fault, parameters of the fault and the day and time when the fault first occurred.

The data fitting system calculates and compares the best possible fit of current 1 error (e_{i1}) and current 2 error (e_{i2}) of the on-line AMB system with the reference current 1 (e_{i1_ref}) and reference current 2 (e_{i2_ref}) of the historical fault database. The data fitting system sends the number of the dataset (N) with the closest fit and the accuracy of the fit (A_{fit}) to the diagnostic system.

The historical fault database provides the diagnostic system with the type of fault (F_{data}). The output is displayed as a percentage fit to a specific dataset and the corresponding fault in the dataset. Each time the identification system recalculates the frequency the parameters A_e_1, B_e_1, C_e_1 and D_e_1 are saved as the output parameters of the fault.

The amplitude of the frequency pattern error (A_B) is obtained by comparing pattern 1 error (e_{1_pat}) and pattern 2 error (e_{2_pat}) with the maximum current output of the power amplifiers ($PA1_{max}$ and $PA2_{max}$). This index provides the diagnostic subsystem with the current state of the rotor. The current state of the rotor is divided into four sections: 1) good working condition, where $e_{1\_pat} < (0.2)\cdot PA1_{max}$; 2) fault in system, where $(0.2)\cdot PA1_{max} \; e_{1\_pat} < (0.45)\cdot PA1_{max}$; 3) critical state, where $(0.45)\cdot PA1_{max} \; e_{1\_pat} \; (0.7)\cdot PA1_{max}$ and 4) system shutdown where $e_{1\_pat} > (0.7)\cdot PA1_{max}$. The same rules apply for e_{2_pat} and $PA2_{max}$.

The side and axis with the largest current error indicates where the fault causes the most damage. The exact time when the fault first occurred is saved and displayed. The running time (t_r) is used to calculate the exact time.

Figure 16 displays data fitting where the frequency of the fault changed from the low frequency area to the high

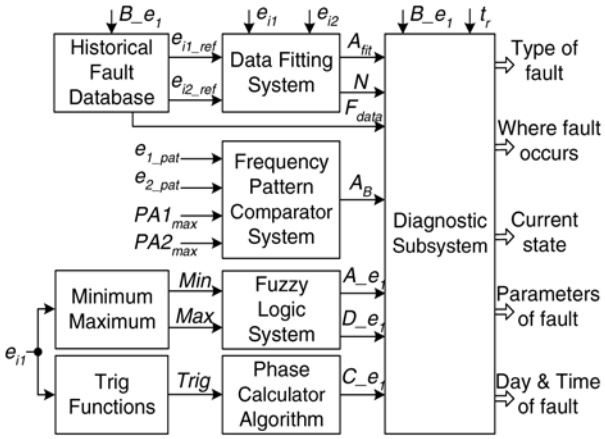

Figure 15: Fault identification system.

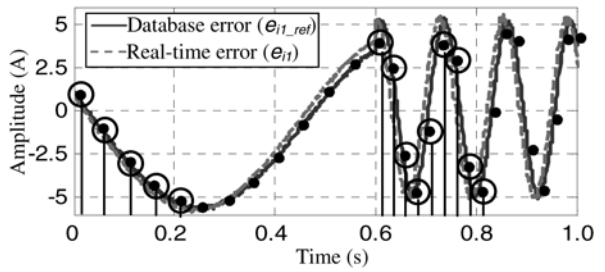

Figure 16: Data fitting of a low frequency fault with sudden change to a high frequency fault.

frequency area. The solid lines represent the historical database error (e_{i1_ref}) from the water cooling AMB pump and the dashed lines represent the real-time error (e_{i1}) from the double radial AMB system. The sampling time of the parameters was increased when the frequency entered the high frequency area. Sampling (shown by the markers) of the parameters is performed by the data fitting system.

Figure 17 provides the fuzzy membership functions for the maximum error (*MAX*) and minimum error (*MIN*). *MAX* refers to the maximum error over a period of time. The maximum block identifies the position of the largest element in each column of the current error (e_{i1}) over a period of time.

MIN refers to the minimum error over a period of time. The minimum block identifies the position of the smallest element in each column of the current error over a period

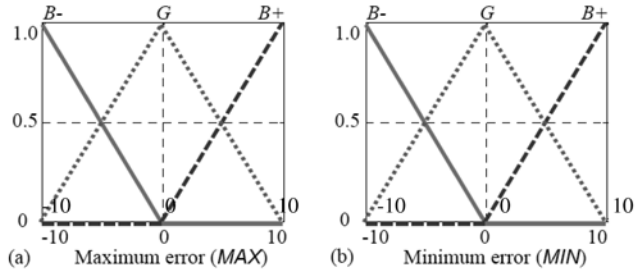

Figure 17: Fuzzy membership functions for (a) the maximum error (*MAX*) and (b) the minimum error (*MIN*).

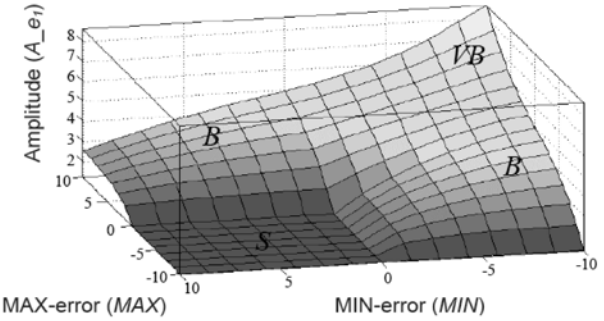

Figure 18: Fuzzy surface plot for amplitude A_e_1.

of time. Fuzzification is performed by using the overlapping fuzzy sets bad negative (*B*-), good (*G*) and bad positive (*B*+).

Table II: Rule matrix for amplitude (A_e_1) and offset (D_e_1)

A_e_1, D_e_1		*MAX*		
		B+	*G*	*B-*
MIN	*B+*	*S, P*	*S, M*	*S, M*
	G	*VB, P*	*S, M*	*S, M*
	B-	*B, M*	*VB, N*	*S, N*

The basic rule for using the features (*MAX* and *MIN*) is: IF *MAX* AND *MIN* THEN A_e_1. The same rule applies for variable D_e_1. Table II provides the rule matrix for the amplitude A_e_1 and offset D_e_1.

The fuzzy surface plots for the amplitude (A_e_1) and the offset (D_e_1) are shown in Figures 18 and 19, respectively. Defuzzification of the fuzzy membership functions A_e_1 and D_e_1 are performed by using the overlapping fuzzy sets small (*S*), big (*B*) and very big (*VB*) and negative (*N*), middle (*M*) and positive (*P*), respectively.

A screenshot of the fault identification program written in MATLAB® is shown in Figure 25. This program performs the calculations and displays the output of the identification system.

4. HARDWARE SETUP

Discrete sampling of the displacement and current signals of the physical AMB system was done by means of the dSPACE® 1104 controller board, equipped with a DSP

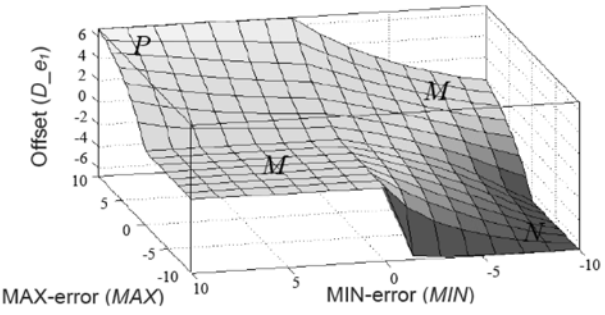

Figure 19: Fuzzy surface plot for offset D_e_1.

TMS320F240 from Texas Instruments. A user-interface was created in Controldesk® to perform data acquisition on the physical system.

Due to the complexity of the control, detection and correction system, the dSPACE® controller was not able to handle all the instructions and real-time errors occurred. This problem was solved by implementing two dSPACE® 1104 controller boards, one for each axes of the magnetic bearing. A roller bearing was installed on the right side of the rotor, which increased the sampling time of the DSP, since only one side has to be suspended.

The vibration force calculations, speed sensor calculations and current masking process were performed by the left dSPACE® controller and communicated to the other dSPACE® controller via serial communication. The application of the vibration forces and diagnosis and correction system calculations were performed by the right dSPACE® controller. Figure 20 shows the hardware setup with the dSPACE® controllers.

During the investigation of the current signals of the double radial AMB system, it became evident that synchronous vibrations were introduced by the roller bearing when the rotor was rotating. These vibrations were therefore integrated into the current masking and correctional pattern calculation process of the fault detection and diagnosis systems (discussed in Sections 3.2 and 3.3).

Figure 21 shows the masked current (i_{1_mask}) and the actual current (i_1) during the practical implementation phase. The no fault current (i_{1_mask}) is subtracted from the fault current (i_{1_fault}) to provide the current error (e_{i1}). The amplitude of the current (i_1) and the frequency (ω) obtained from the rotational speed of the rotor were used as scaling factors for the masked current. When the amplitude (i_1) and frequency (ω) increased, the amplitudes and frequencies of the individual signals in the masked current were also increased.

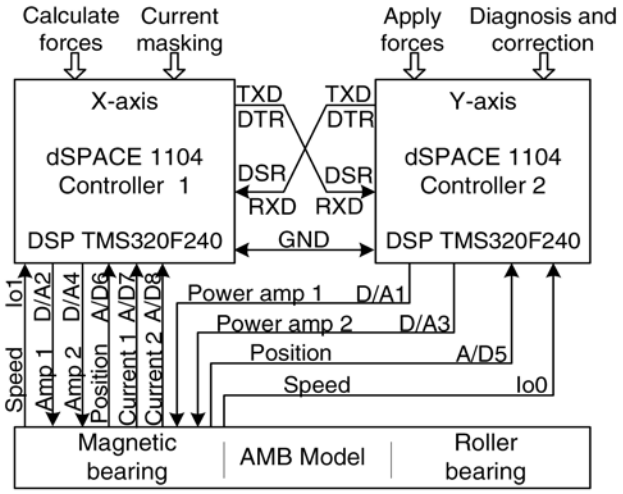

Figure 20: Hardware setup with the dSPACE® controllers.

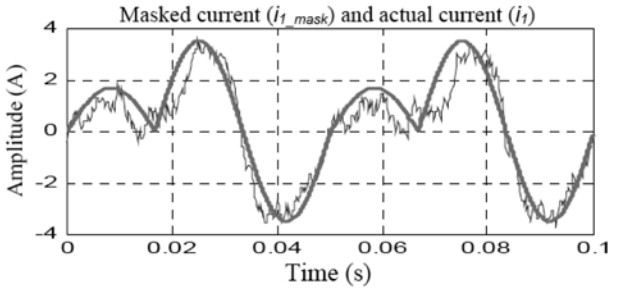

Figure 21: Current masking during practical implementation.

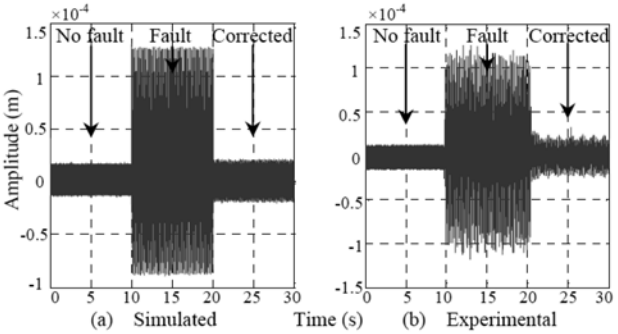

Figure 22: System with low frequency vibration force.

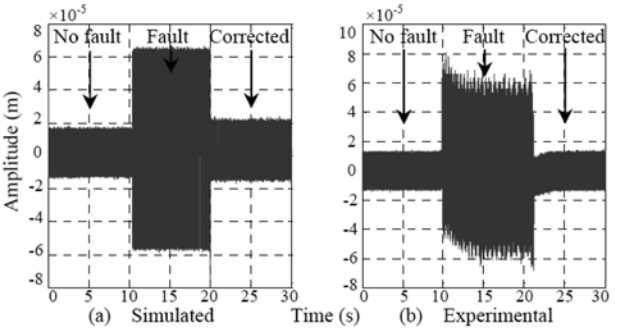

Figure 23: System with medium frequency vibration force.

5. SIMULATION VERIFICATION

This section provides the simulated and experimental results of the double radial AMB test rack, with low, medium and high frequency vibration forces.

During the simulation phase of this project the carrier frequency was chosen at 104.7 rad/sec (1000 rpm) and faults were simulated by applying the vibration force (f_4) files to the system to see how the diagnosis and correction system reacts.

During the practical implementation phase of this project, the rotor was held constant at 1000 rpm and vibration forces were simulated by implementing the reference current fault (i_f) files to the system to see how the diagnosis and correction reacts.

Figures 22 and 23 show the actual displacement (x_p) of the AMB system with low and medium frequency vibration forces, respectively.

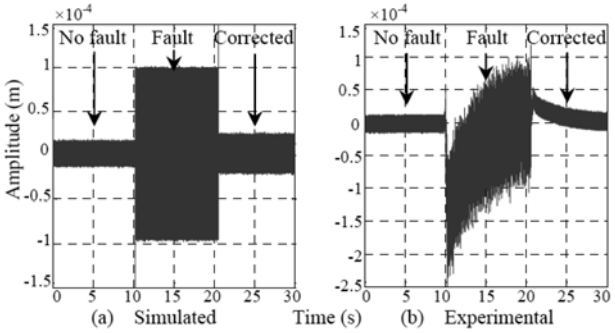

Figure 24: System with high frequency vibration force.

Figure 24 shows the actual displacement of the AMB system with a high frequency vibration force. The system was designed to simulate and capture the actual displacement of the simulation and practical AMB models (shown in Figure 5) without any vibration force for the first 10 seconds, thereafter to induce the fault and activate the detection, diagnosis and correction system after 20 seconds.

From the above figures it can be seen that the practical AMB system provides even better results than the simulation AMB model.

6. CONCLUSION

The work presented in this paper focused on current analysis, correction and identification of vibration forces on the rotor of an AMB system.

The experimental results of the double radial AMB test rack correlated with the simulated results and vibration forces were corrected or minimised to a stable working condition.

The pattern construction subsystem was able to construct new and combination patterns and the diagnosis and correction system was able to use these patterns to correct vibration forces.

The fault identification system was able to calculate the exact type of fault, where the fault occurred, the current state of the fault, the parameters of the fault and the exact day and time when the fault first occurred.

The current limit of the power amplifiers and the run-time of the DSP processors were the two main limitations of this project. During normal operation of the double radial AMB, the power amplifiers require 4 ampere, which only leaves 6 ampere for fault application and correctional purposes.

Due to the complexity of the detection, diagnosis and correctional system, a lot of processing time was required, which caused run-time errors during real-time implementation on the dSPACE® controller. This problem was solved by implementing an additional dSPACE® controller.

The methods and implementation of predictive simulation, model validation and test implementation were shown here to be useful for detection, diagnosis and correction of vibration forces on the rotor of the AMB system.

ACKNOWLEDGMENTS

The authors wish to thank the Institute for Process Technology, Automation and Measurement Technology (IPM) at the University of Applied Sciences Zittau/Görlitz in Germany for making it possible to work on the 250 kW water cooling AMB pump.

7. REFERENCES

[1] R. Herzog, P. Buhler, C. Gahler and R. Larsonneur: "Unbalance compensation using generalized notch filters in the multivariable feedback of magnetic bearings", *IEEE Transactions on Control Systems Technology*, Vol. 4, No. 5, pp. 580-586, Sep. 1996.

[2] M. Ahrens, L. Kucera and R. Larsonneur: "Performance of a magnetically suspended flywheel energy storage device", *IEEE Transactions on Control Systems Technology*, Vol. 4, No. 5, pp. 494-502, Sep. 1996.

[3] F. Matsumura, T. Namerikawa, K. Hagiwara and M. Fujita: "Application of gain scheduled $H\infty$ robust controllers to a magnetic bearing", *IEEE Transactions on Control Systems Technology*, Vol. 4, No. 5, pp. 484-493, Sep. 1996.

[4] A. Duyar, V. Eldem, W. Merrill and T.H. Guo: "Fault detection and diagnosis in propulsion system:

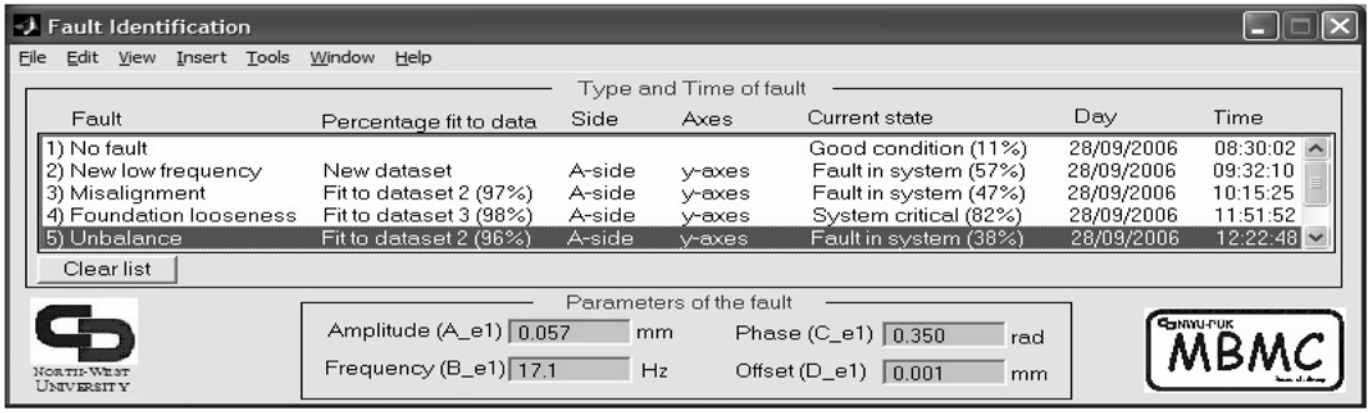

Figure 25: Screenshot of the fault identification program.

A fault parameter estimation approach", *J. Guidance, Contr., Dynam.*, Vol. 17, No. 1, pp. 104-108, 1994.

[5] P.M. Frank: "Fault diagnosis in dynamic systems using analytical and knowledge-based redundancy - A survey and some new results", *Automatica*, Vol. 26, No. 3, pp. 459-474, 1990.

[6] R. Isermann: "Fault diagnosis of machine via parameter estimation and knowledge processing - Tutorial paper", *Automatica*, Vol. 29, No. 4, pp. 815-835, 1993.

[7] R. Herzog, P. Buhler, C. Gahler and R. Larsonneur: "Unbalance compensation using generalized notch filters in the multivariable feedback of magnetic bearings", *IEEE Transactions on Control Systems Technology*, Vol. 4, Issue 5, pp. 580-586, Sep. 1996.

[8] J.T. Marshall: "A multi-point measurement technique for the enhancement of force measurement with active magnetic bearings (AMB)", *Faculty of the Virginia Polytechnic Institute and State University*, Blacksburg, Virginia, May 2001.

[9] W.J. Staszewski: "Gearbox vibration diagnostics-an overview", *The 8th International Congress on Condition Monitoring and Diagnostic Engineering Management (COMADEM-96)*, Sheffield, England, July 1996.

[10] D.E. Newland: *An introduction to random vibrations, spectral & wavelet analysis*, Longman Scientific & Technical, 3rd Ed., 1993.

[11] M. Chiollaz and B. Frave: "Engine noise characterization with Wigner-Ville time-frequency analysis", *Mechanical Systems and Signal Processing*, Vol. 7 No. 5, pp. 375-400, 1993.

[12] J. Ville: "Theorie et applications de la notion de signal analytique", *Cables et Transmissions*, Vol. 2, No. 1, pp. 61-74, 1948.

[13] R.N. Bracewell: *The Fourier transform and its applications*, 3rd Ed., New York: McGraw-Hill, 1999.

[14] L. Cohen: "Time-frequency distributions - A review", *Proceedings of the IEEE*, Vol. 77, No. 7, pp. 941-981, 1989.

[15] B. Boashash: *In advances in spectrum analysis and array processing*, Englewood Cliffs, New Jersey: Prentice Hall, 1991.

APPENDIX

Figure 25 shows a screenshot of the fault identification program written in MATLAB®. This program calculates and displays the parameters of the fault identification system of Figure 15. Faults are calculated and displayed as a specific type (misalignment, foundation looseness, unbalance or as otherwise specified in the historical fault database), percentage fit to a specific dataset, side where the fault occurs (A-side or B-side), axes where the fault occurs (x, y or z-axes), current state of the fault (good, fault, critical or shutdown) as well as the actual error percentage of the fault and day and time when the fault first occurred. The parameters (amplitude, frequency, phase and offset) of the fault are also shown.

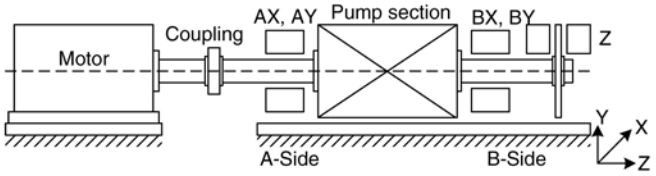

Figure 26: Water cooling AMB pump.

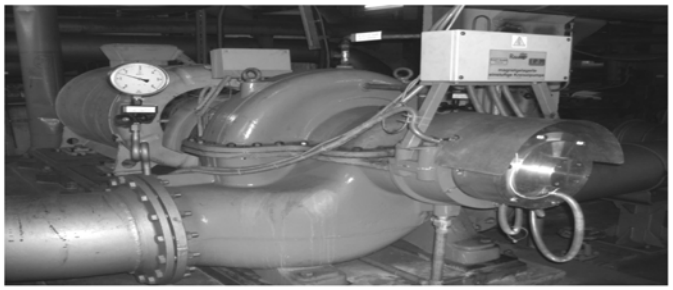

Figure 27: Water cooling AMB pump (physical system).

A diagram and picture of the fully suspended 250 kW water cooling AMB pump can be seen in Figures 26 and 27, respectively. Current condition monitoring was performed over a period of 3 years to obtain historical fault data on the water cooling AMB pump.

Due to technical aspects it was not possible to make any changes to the water cooling AMB pump.

The specifications of the water cooling AMB pump can be seen in Table III. A picture of the double radial AMB system can be seen in Figure 28. Table IV provides the specifications of the double radial AMB test rack.

Table III: Specifications of the water cooling AMB pump

Parameter	Specification		Unit	Description
	Axial	Radial		
F	12000	7500	N	Load capacity
x_{pn}	0.8	0.4	mm	Nominal air gap
i_0	6	6	A	Bias current
i_1	15	15	A	Control current

Table IV: Specifications of the double radial AMB system

Parameter	Specification	Unit	Description
F_{max}	500	N	Maximum load capacity
x_{pn}	0.6	mm	Nominal air gap
i_0	3	A	Bias current
i_1	10	A	Control current

Figure 28: Double radial AMB (physical system).